

Contents lists available at ScienceDirect

Physics Letters B

www.elsevier.com/locate/physletbFinal COMPASS results on the deuteron spin-dependent structure function g_1^d and the Bjorken sum rule

C. Adolph^h, M. Aghasyan^y, R. Akhunzyanov^g, M.G. Alexeev^{aa}, G.D. Alexeev^g, A. Amoroso^{aa,ab}, V. Andrieux^{ac,u}, N.V. Anfimov^g, V. Anosov^g, K. Augsten^{g,s}, W. Augustyniak^{ad}, A. Austregesilo^p, C.D.R. Azevedo^a, B. Badełek^{ae}, F. Balestra^{aa,ab}, M. Ball^c, J. Barth^d, R. Beck^c, Y. Bedfer^u, J. Bernhard^{m,j}, K. Bicker^{p,j}, E.R. Bielert^j, R. Birsa^y, M. Bodlak^r, P. Bordalo^{l,1}, F. Bradamante^{x,y}, C. Braun^h, A. Bressan^{x,y}, M. Bücheleⁱ, W.-C. Chang^v, C. Chatterjee^f, M. Chiosso^{aa,ab}, I. Choi^{ac}, S.-U. Chung^{p,2}, A. Cicuttin^{z,y}, M.L. Crespo^{z,y}, Q. Curiel^u, S. Dalla Torre^y, S.S. Dasgupta^f, S. Dasgupta^{x,y}, O.Yu. Denisov^{ab,*}, L. Dhara^f, S.V. Donskov^t, N. Doshita^{ag}, Ch. Dreisbach^p, V. Duic^x, W. Dünnweber³, M. Dziewiecki^{af}, A. Efremov^g, P.D. Eversheim^c, W. Eyrich^h, M. Faessler³, A. Ferrero^u, M. Finger^r, M. Finger jr.^r, H. Fischerⁱ, C. Franco^l, N. du Fresne von Hohenesche^m, J.M. Friedrich^p, V. Frolov^{g,j}, E. Fuchey^u, F. Gautheron^b, O.P. Gavrichtchouk^g, S. Gerassimov^{o,p}, J. Giarra^m, F. Giordano^{ac}, I. Gnesi^{aa,ab}, M. Gorzellik^{i,4}, S. Grabmüller^p, A. Grasso^{aa,ab}, M. Grosse Perdekamp^{ac}, B. Grube^p, T. Grussenmeyerⁱ, A. Guskov^g, F. Haas^p, D. Hahne^d, G. Hamar^{x,y}, D. von Harrach^m, F.H. Heinsiusⁱ, R. Heitz^{ac}, F. Herrmannⁱ, N. Horikawa^{q,5}, N. d'Hose^u, C.-Y. Hsieh^{v,6}, S. Huber^p, S. Ishimoto^{ag,7}, A. Ivanov^{aa,ab}, Yu. Ivanshin^g, T. Iwata^{ag}, V. Jary^s, R. Joosten^c, P. Jörgⁱ, E. Kabuß^m, A. Kerbizi^{x,y}, B. Ketzer^c, G.V. Khaustov^t, Yu.A. Khokhlov^{t,8,9}, Yu. Kisselev^g, F. Klein^d, K. Klimaszewski^{ad}, J.H. Koivuniemi^b, V.N. Kolosov^t, K. Kondo^{ag}, K. Königsmannⁱ, I. Konorov^{o,p}, V.F. Konstantinov^t, A.M. Kotzinian^{aa,ab}, O.M. Kouznetsov^g, M. Krämer^p, P. Kremserⁱ, F. Krinner^p, Z.V. Kroumchtein^{g,23}, Y. Kulinich^{ac}, F. Kunne^u, K. Kurek^{ad}, R.P. Kurjata^{af}, A.A. Lednev^{t,23}, A. Lehmann^h, M. Levillain^u, S. Levorato^y, Y.-S. Lian^{v,10}, J. Lichtenstadt^w, R. Longo^{aa,ab}, A. Maggiora^{ab}, A. Magnon^{ac}, N. Makins^{ac}, N. Makke^{x,y}, G.K. Mallot^{j,*}, B. Marianski^{ad}, A. Martin^{x,y}, J. Marzec^{af}, J. Matoušek^{r,y}, H. Matsuda^{ag}, T. Matsudaⁿ, G.V. Meshcheryakov^g, M. Meyer^{ac,u}, W. Meyer^b, Yu.V. Mikhailov^t, M. Mikhasenko^c, E. Mitrofanov^g, N. Mitrofanov^g, Y. Miyachi^{ag}, A. Nagaytsev^g, F. Nerling^m, D. Neyret^u, J. Nový^{s,j}, W.-D. Nowak^m, G. Nukazuka^{ag}, A.S. Nunes^l, A.G. Olshevsky^g, I. Orlov^g, M. Ostrick^m, D. Panziera^{ab,11}, B. Parsamyan^{aa,ab}, S. Paul^p, J.-C. Peng^{ac}, F. Pereira^a, M. Pešek^r, D.V. Peshekhonov^g, N. Pierre^{m,u}, S. Platchkov^u, J. Pochodzalla^m, V.A. Polyakov^t, J. Pretz^{d,12}, M. Quaresima^l, C. Quintans^l, S. Ramos^{l,1}, C. Regaliⁱ, G. Reicherz^b, C. Riedl^{ac}, M. Roskot^r, N.S. Rossiyskaya^g, D.I. Ryabchikov^{t,9}, A. Rybnikov^g, A. Rychter^{af}, R. Salac^s, V.D. Samoylenko^t, A. Sandacz^{ad}, C. Santos^y, S. Sarkar^f, I.A. Savin^g, T. Sawada^v, G. Sbrizzai^{x,y}, P. Schiavon^{x,y}, K. Schmidt^{i,4}, H. Schmieden^d, K. Schönning^{j,13}, E. Seder^{u,y}, A. Selyunin^g, L. Silva^l, L. Sinha^f, S. Sirtlⁱ, M. Slunecka^g, J. Smolik^g, A. Srnka^e, D. Steffen^{j,p}, M. Stolarski^l, O. Subrt^{j,s}, M. Sulc^k, H. Suzuki^{ag,5}, A. Szabelski^{ad,y}, T. Szameitat^{i,4}, P. Sznajder^{ad}, S. Takekawa^{aa,ab}

* Corresponding authors.

E-mail addresses: oleg.denisov@cern.ch (O.Yu. Denisov), gerhard.mallot@cern.ch (G.K. Mallot), malte.christian.wilfert@cern.ch (M. Wilfert).

M. Tasevsky^g, S. Tassarò^y, F. Tassarotto^y, F. Thibaud^u, A. Thiel^c, F. Tosello^{ab}, V. Tskhay^o,
S. Uhl^p, A. Vauth^j, J. Veloso^a, M. Virius^s, J. Vondra^s, S. Wallner^p, T. Weisrock^m,
M. Wilfert^{m,*}, R. Windmolders^d, J. ter Wolbeek^{i,4}, K. Zaremba^{af}, P. Zavada^g,
M. Zavertyaev^o, E. Zemlyanichkina^g, N. Zhuravlev^g, M. Ziembicki^{af}, A. Zink^h,

^a University of Aveiro, Dept. of Physics, 3810-193 Aveiro, Portugal

^b Universität Bochum, Institut für Experimentalphysik, 44780 Bochum, Germany^{14,15}

^c Universität Bonn, Helmholtz-Institut für Strahlen- und Kernphysik, 53115 Bonn, Germany¹⁴

^d Universität Bonn, Physikalisches Institut, 53115 Bonn, Germany¹⁴

^e Institute of Scientific Instruments, AS CR, 61264 Brno, Czech Republic¹⁶

^f Matrivani Institute of Experimental Research & Education, Calcutta-700 030, India¹⁷

^g Joint Institute for Nuclear Research, 141980 Dubna, Moscow region, Russia¹⁸

^h Universität Erlangen–Nürnberg, Physikalisches Institut, 91054 Erlangen, Germany¹⁴

ⁱ Universität Freiburg, Physikalisches Institut, 79104 Freiburg, Germany^{14,15}

^j CERN, 1211 Geneva 23, Switzerland

^k Technical University in Liberec, 46117 Liberec, Czech Republic¹⁶

^l LIP, 1000-149 Lisbon, Portugal¹⁹

^m Universität Mainz, Institut für Kernphysik, 55099 Mainz, Germany¹⁴

ⁿ University of Miyazaki, Miyazaki 889-2192, Japan²⁰

^o Lebedev Physical Institute, 119991 Moscow, Russia

^p Technische Universität München, Physik Dept., 85748 Garching, Germany^{14,3}

^q Nagoya University, 464 Nagoya, Japan²⁰

^r Charles University in Prague, Faculty of Mathematics and Physics, 18000 Prague, Czech Republic¹⁶

^s Czech Technical University in Prague, 16636 Prague, Czech Republic¹⁶

^t State Scientific Center Institute for High Energy Physics of National Research Center ‘Kurchatov Institute’, 142281 Protvino, Russia

^u IRFU, CEA, Université Paris-Saclay, 91191 Gif-sur-Yvette, France¹⁵

^v Academia Sinica, Institute of Physics, Taipei 11529, Taiwan

^w Tel Aviv University, School of Physics and Astronomy, 69978 Tel Aviv, Israel²¹

^x University of Trieste, Dept. of Physics, 34127 Trieste, Italy

^y Trieste Section of INFN, 34127 Trieste, Italy

^z Abdus Salam ICTP, 34151 Trieste, Italy

^{aa} University of Turin, Dept. of Physics, 10125 Turin, Italy

^{ab} Torino Section of INFN, 10125 Turin, Italy

^{ac} University of Illinois at Urbana-Champaign, Dept. of Physics, Urbana, IL 61801-3080, USA

^{ad} National Centre for Nuclear Research, 00-681 Warsaw, Poland²²

^{ae} University of Warsaw, Faculty of Physics, 02-093 Warsaw, Poland²²

^{af} Warsaw University of Technology, Institute of Radioelectronics, 00-665 Warsaw, Poland²²

^{ag} Yamagata University, Yamagata 992-8510, Japan²⁰

ARTICLE INFO

Article history:

Received 15 December 2016

Received in revised form 3 March 2017

Accepted 10 March 2017

Available online 16 March 2017

Editor: M. Doser

Keywords:

COMPASS

Deep inelastic scattering

Spin

Structure function

Parton helicity distributions

ABSTRACT

Final results are presented from the inclusive measurement of deep-inelastic polarised-muon scattering on longitudinally polarised deuterons using a ⁶LiD target. The data were taken at 160 GeV beam energy and the results are shown for the kinematic range $1(\text{GeV}/c)^2 < Q^2 < 100(\text{GeV}/c)^2$ in photon virtuality, $0.004 < x < 0.7$ in the Bjorken scaling variable and $W > 4\text{GeV}/c^2$ in the mass of the hadronic final state. The deuteron double-spin asymmetry A_1^d and the deuteron longitudinal-spin structure function g_1^d are presented in bins of x and Q^2 . Towards lowest accessible values of x , g_1^d decreases and becomes consistent with zero within uncertainties. The presented final g_1^d values together with the recently published final g_1^p values of COMPASS are used to again evaluate the Bjorken sum rule and perform the QCD fit to the g_1 world data at next-to-leading order of the strong coupling constant. In both cases, changes in central values of the resulting numbers are well within statistical uncertainties. The flavour-singlet axial charge a_0 , which is identified in the $\overline{\text{MS}}$ renormalisation scheme with the total contribution of quark helicities to the nucleon spin, is extracted at next-to-leading order accuracy from only the COMPASS deuteron data: $a_0(Q^2 = 3(\text{GeV}/c)^2) = 0.32 \pm 0.02_{\text{stat}} \pm 0.04_{\text{syst}} \pm 0.05_{\text{evol}}$. Together with the recent results on the proton spin structure function g_1^p , the results on g_1^d constitute the COMPASS legacy on the measurements of g_1 through inclusive spin-dependent deep inelastic scattering.

© 2017 The Author(s). Published by Elsevier B.V. This is an open access article under the CC BY license (<http://creativecommons.org/licenses/by/4.0/>). Funded by SCOAP³.

¹ Also at Instituto Superior Técnico, Universidade de Lisboa, Lisbon, Portugal.

² Also at Dept. of Physics, Pusan National University, Busan 609-735, Republic of Korea and at Physics Dept., Brookhaven National Laboratory, Upton, NY 11973, USA.

³ Supported by the DFG cluster of excellence ‘Origin and Structure of the Universe’ (www.universe-cluster.de).

⁴ Supported by the DFG Research Training Group Programmes 1102 and 2044.

⁵ Also at Chubu University, Kasugai, Aichi 487-8501, Japan.

⁶ Also at Dept. of Physics, National Central University, 300 Jhongda Road, Jhongli 32001, Taiwan.

⁷ Also at KEK, 1-1 Oho, Tsukuba, Ibaraki 305-0801, Japan.

⁸ Also at Moscow Institute of Physics and Technology, Moscow Region, 141700, Russia.

⁹ Supported by Presidential grant NSh-999.2014.2.

¹⁰ Also at Dept. of Physics, National Kaohsiung Normal University, Kaohsiung County 824, Taiwan.

1. Introduction

About a quarter of a century ago, measurements of the spin-dependent structure function g_1^p by EMC [1] led to the very surprising result that the quark spin contribution to the nucleon spin of $1/2$ might be very small or even vanishing, albeit with large experimental uncertainties. This result initiated enormous experimental and theoretical activities to study the spin structure of the nucleon. In subsequent measurements by SMC [2], an upgraded apparatus was used to confirm with better precision that only about one third of the spin of the nucleon is made up by quark spins. This observation is supported by recent lattice QCD simulations [3].

In the last two decades, several new experiments were set up at various laboratories to study the longitudinal spin structure of the nucleon in even more detail. These experiments included COMPASS at CERN using the CERN SPS muon beam line at energies 160 GeV and 200 GeV, HERMES at DESY using the 27.5 GeV electron beam of HERA, many experiments at the 6 GeV electron beam of Jefferson Laboratory, as well as PHENIX and STAR at the proton-proton collider RHIC with a centre of mass energy of 270 GeV. Except for the latter two, in all other experiments the longitudinal spin structure of the nucleon was studied by inclusive measurements of spin-dependent deep-inelastic lepton-nucleon scattering (DIS) using longitudinally polarised beams and targets, in particular by measuring double-spin cross-section asymmetries. More details can be found in recent reviews, see e.g. Ref. [4].

The measured value of the parton helicity contribution to the proton spin is very sensitive to the minimal experimental accessible value of the Bjorken- x variable. Therefore measurements at low x are crucial to understand the spin structure of the nucleon. According to theoretical expectations, new contributions to the DGLAP QCD evolution, e.g. double logarithmic terms [5,6], may be important in this region. Perturbative QCD is considered to be applicable for values of Q^2 as low as $1 (\text{GeV}/c)^2$. At COMPASS, using a 160 GeV muon beam, this corresponds to a minimal value of x equal to 0.004.

In this Letter, results are presented on the longitudinal double-spin asymmetry A_1^d and the longitudinal spin structure function g_1^d of the deuteron. They are obtained from data taken in 2006 with the CERN 160 GeV longitudinally polarised muon beam and a longitudinally polarised ^6LiD target. These results are described and compared to those published earlier [7] for the 2002–2004 data. The analysis of the combined 2002–2006 data yields the final COMPASS results on A_1^d and g_1^d . Moreover, the combined data set analysed in this work extends to high Q^2 values that were for-

merly only reached by SMC, thereby improving considerably the statistical accuracy. Together with the results on the proton spin structure function g_1^p [8,9], the results for g_1^d constitute the COMPASS legacy on the measurements of g_1 through inclusive DIS.

The Letter is organised as follows. Experimental set-up and data analysis are described in Sect. 2. The physics context of the analysis and details on the calculation of asymmetries are given in Sect. 3. In Sect. 4, the results are presented and interpreted. Summary and conclusions are given in Sect. 5. The reader is referred to Ref. [10] for a detailed description of the analysis.

2. Experimental set-up and data analysis

The COMPASS spectrometer used in 2002–2004 and the upgrades of the polarised target solenoid and the RICH detector performance in 2005 are described in detail in Ref. [12]. In 2006 the target material was ^6LiD contained in three cells instead of two. They were located along the beam one after the other and had a diameter of 3 cm. The two outermost cells had a length of 30 cm and the central cell was 60 cm long. The deuteron polarisation in ^6LiD was $P_T \approx 0.52$, and the direction of the target polarisation in the outer cells was opposite to that of the central one. The polarisation direction was inverted on a regular basis by rotating the direction of the target solenoid magnetic field. During the data taking, the direction of the polarisation with respect to the solenoid field was inverted by repolarisation in opposite directions keeping the solenoid field unchanged. The tertiary M2 beam of the CERN SPS delivered a naturally polarised muon beam with a polarisation of $P_B \approx 0.8$. The nominal momentum was 160 GeV/c with a momentum spread of 5%. Momentum and trajectory of each beam particle were measured by sets of scintillator hodoscopes, scintillating fibre and silicon detectors. The particles produced in an interaction were detected in a two-stage open forward spectrometer with large momentum and angular acceptance. Each stage contained a dipole magnet complemented with various tracking detectors (scintillating fibre detectors, micropattern gaseous detectors, multiwire proportional chambers, drift chambers, straw detectors), as well as hadron and electromagnetic calorimeters. In the first stage, a RICH detector was available for hadron identification. Scattered muons were detected by drift tube planes and multiwire proportional chambers located behind iron and concrete absorbers. Two types of triggers were used in this analysis. The “inclusive” trigger was based on a signal from a combination of hodoscope signals from the scattered muon. The “semi-inclusive” triggers required an energy deposition in one of the calorimeters with an optional coincidence with the inclusive trigger.

Events with a reconstructed interaction point in one of the three target cells are selected requiring at least a reconstructed incoming muon and a scattered muon. The measured momentum of the incident muon has to be in the range $140 \text{ GeV}/c < p_B < 180 \text{ GeV}/c$, and the extrapolated beam track has to cross all target cells to equalise the flux through them. The amount of unpolarised material surrounding the polarised material is minimised by a radial cut on the vertex position of $r < 1.4 \text{ cm}$. The scattered muon is identified by requiring that it has passed more than 30 radiation lengths and points to the hodoscope that triggered the event. In addition, kinematic constraints on the scattering process are applied. A photon virtuality of $Q^2 > 1 (\text{GeV}/c)^2$ is required and the relative virtual-photon energy has to be in the range $0.1 < y < 0.9$. Here, the lower limit removes events that are difficult to reconstruct, and the upper limit removes events, the kinematics of which are dominated by radiative effects. These selection criteria

¹¹ Also at University of Eastern Piedmont, 15100 Alessandria, Italy.

¹² Present address: RWTH Aachen University, III. Physikalisches Institut, 52056 Aachen, Germany.

¹³ Present address: Uppsala University, Box 516, 75120 Uppsala, Sweden.

¹⁴ Supported by the German Bundesministerium für Bildung und Forschung.

¹⁵ Supported by EU FP7 (HadronPhysics3, Grant Agreement number 283286).

¹⁶ Supported by Czech Republic MEYS Grant LG13031.

¹⁷ Supported by SAIL (CSR), Govt. of India.

¹⁸ Supported by CERN-RFBR Grant 12-02-91500.

¹⁹ Supported by the Portuguese FCT – Fundação para a Ciência e Tecnologia, COMPETE and QREN, Grants CERN/FP 109323/2009, 116376/2010, 123600/2011 and CERN/FIS-NUC/0017/2015.

²⁰ Supported by the MEXT and the JSPS under the Grants No. 18002006, No. 20540299 and No. 18540281; Daiiko Foundation and Yamada Foundation.

²¹ Supported by the Israel Academy of Sciences and Humanities.

²² Supported by the Polish NCN Grant 2015/18/M/ST2/00550.

²³ Deceased.

lead to the kinematic range $0.004 < x < 0.7$ and to a minimal mass of the hadronic final state of $W > 4 \text{ GeV}/c^2$. The final sample consists of 46 million events.

3. Asymmetry calculation

The longitudinal double-spin asymmetry for one-photon exchange in inclusive DIS on the deuteron, $\mu d \rightarrow \mu' X$, is defined as a function of x and Q^2 as follows:

$$A_1^d = \frac{\sigma_0^T - \sigma_2^T}{2\sigma^T}. \quad (1)$$

Here, σ_J^T is the γ^* -deuteron absorption cross section for total spin projection J in the direction of the virtual photon γ^* and $\sigma^T = (\sigma_0^T + \sigma_1^T + \sigma_2^T)/3$ the deuteron photoabsorption cross section for transverse virtual photons. This asymmetry is derived from the asymmetry between the cross sections for parallel and antiparallel oriented longitudinal spins of beam particle and target nucleon²⁴:

$$A_{LL}^d = \frac{\sigma^{\uparrow\downarrow} - \sigma^{\uparrow\uparrow}}{\sigma^{\uparrow\downarrow} + \sigma^{\uparrow\uparrow}} = D(A_1^d + \eta A_2^d). \quad (2)$$

Here, also the contribution from the transverse spin asymmetry A_2^d is taken into account. The factors

$$\eta = \frac{\gamma(1-y-\gamma^2 y^2/4 - y^2 m^2/Q^2)}{(1+\gamma^2 y/2)(1-y/2) - y^2 m^2/Q^2} \quad (3)$$

and

$$D = \frac{y((1+\gamma^2 y/2)(2-y) - 2y^2 m^2/Q^2)}{y^2(1-2m^2/Q^2)(1+\gamma^2) + 2(1+R)(1-y-\gamma^2 y^2/4)} \quad (4)$$

depend only on the kinematics of the process, with $\gamma = 2Mx/\sqrt{Q^2}$. The symbols m and M denote the mass of the muon and the nucleon, respectively. The factor R in the depolarisation factor D represents the ratio of the cross sections for the absorption of a longitudinally and a transversely polarised photon by a nucleon. In COMPASS kinematics, the factor η and the asymmetry A_2 are both small, and hence the contribution ηA_2 is neglected in the calculation of A_1 and g_1 .

For the calculation of the asymmetry, the number of events in each target cell for both polarisation directions can be expressed as

$$N_i = a_i \phi_i n_i \bar{\sigma} (1 + P_B P_T f D A_1^d), \quad i = o1, c1, o2, c2. \quad (5)$$

Here, a_i is the acceptance, ϕ_i the incoming flux, n_i the number of target nucleons, $\bar{\sigma}$ the spin-averaged cross section and f the dilution factor. There are four equations describing the two solenoid field directions (1, 2) for the combined outer cells (o) and the central cell (c). They are combined into one second-order equation in A_1 for the ratio $(N_{o1} N_{c2})/(N_{o2} N_{c1})$, where acceptance and flux

²⁴ While for a spin-1/2 target the first equality in Eq. (2) is strict, for a spin-1 target there is an extra contribution in the denominator of the asymmetry $A_{LL}^d = \frac{\sigma^{\uparrow\downarrow} - \sigma^{\uparrow\uparrow}}{\sigma^{\uparrow\downarrow} + \sigma^{\uparrow\uparrow} + \sigma^{\uparrow 0}}$, which is connected to the structure function b_1 . This function is expected to be small [13], as also confirmed by a measurement [14], and hence neglected here.

Table 1
Summary for the systematic uncertainty of A_1 .

Beam polarisation	$\Delta P_B/P_B$	5%
Target polarisation	$\Delta P_T/P_T$	5%
Depolarisation factor	$\Delta D(R)/D(R)$	2–3%
Dilution factor	$\Delta f/f$	2–3%
Total	ΔA_1^{mult}	$\approx 0.08 \cdot A_1^d$
False asymmetry	A_{false}	$< 0.75 \cdot \Delta A_1^{\text{stat}}$
Transverse asymmetry	$\eta \cdot A_2^d$	$< 10^{-4}$
Rad. corrections	A^{RC}	$10^{-5} - 10^{-3}$

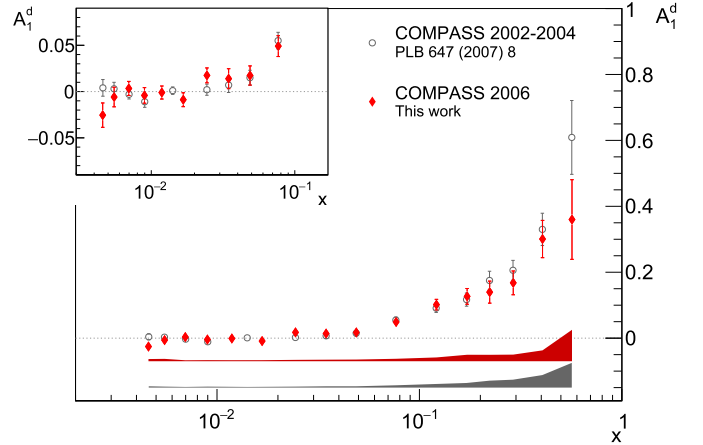


Fig. 1. Comparison between the results on A_1^d obtained from the 2006 data set and the previous results from COMPASS.

cancel. The asymmetry is calculated for periods of stable data taking, which are combined using the weighted mean. In the asymmetry calculation, each event is used with a weight factor in order to minimise the statistical uncertainty:

$$w = P_B f D. \quad (6)$$

Systematic uncertainties are calculated taking into account multiplicative and additive contributions. The multiplicative contribution ΔA_1^{mult} comprises the uncertainties on beam and target polarisations and the uncertainties on depolarisation and dilution factors. The size of each of these contributions is shown in the upper part of Table 1. The lower part of the table shows the additive contributions from i) possible false asymmetries, ii) the neglect of the transverse asymmetry A_2 and iii) the uncertainty on spin-dependent radiative corrections. False asymmetries are investigated using two methods. In one method, possible false asymmetries are studied by calculating the asymmetry between cells with the same polarisation direction, i.e. between both outermost target cells and for the two halves of the central cell. Both asymmetries are found to be consistent with zero. In the other method, “pulls” [15] are used to check for time-dependent effects. Here the asymmetry is calculated for each subsample and compared to the final asymmetry. No significant broadening is observed in these distributions. The statistical limitation of this method leads to an uncertainty between 38% and 75% of the statistical uncertainty. This represents the largest additive contribution.

4. Results

The double-spin asymmetry A_1^d and the spin-dependent structure function g_1^d are calculated in bins of x and Q^2 . In Fig. 1 the results in bins of x obtained from the 2006 data set are compared

to the results from the 2002–2004 data [7], which demonstrates the good agreement between both data sets (the χ^2 probability is 63%). The 2006 data increase the statistics of the 2002–2004 data by approximately 50%. The results from both data sets are combined using the weighted mean. In Fig. 2, the combined COMPASS results on A_1^d are compared to the world data on A_1^d at the measured values of Q^2 . All data sets agree well with one another.

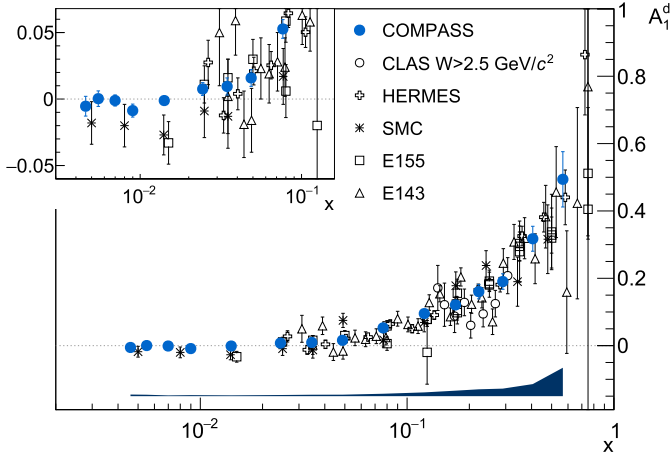


Fig. 2. Comparison between the combined COMPASS results on A_1^d and the world data (CLAS [16], HERMES [17], SMC [2], E155 [18] and E143 [19]). All data points are shown at their measured Q^2 values.

The data confirm the well-known weak Q^2 dependence of the asymmetry. This is also illustrated in Fig. 3, which shows the Q^2 dependence of the COMPASS data for each x bin. No clear dependence on Q^2 is visible in any x bin. The numerical values of $A_1^d(x)$ and $A_1^d(x, Q^2)$ are given in Tables A.1 and A.2 of the appendix.

The spin-dependent structure function g_1^d is calculated from the asymmetry A_1^d using

$$g_1^d(x, Q^2) = \frac{F_2^d(x, Q^2)}{2x(1 + R(x, Q^2))} A_1^d(x, Q^2). \quad (7)$$

The parametrisation of the unpolarised structure function F_2^d is taken from Ref. [2] and the parametrisation of the ratio R is taken from Ref. [20]. The x dependence of the structure function is shown in Fig. 4 together with the results from SMC [2] that were obtained at a higher beam energy of 190 GeV. In the figure, the two COMPASS data points at lowest x are obtained as averages from the four lowest x bins used in this analysis. The systematic uncertainties are shown by bands at the bottom. The COMPASS data do not support large negative values of the structure function at low x , an indication of which may be seen in the SMC data. Instead, g_1^d is compatible with zero for x decreasing towards the lower limit of the measured range.

The new results on the spin-dependent structure function g_1^d , which are shown in Fig. 5 together with the world data in bins of x and Q^2 , constitute the final COMPASS results and hence su-

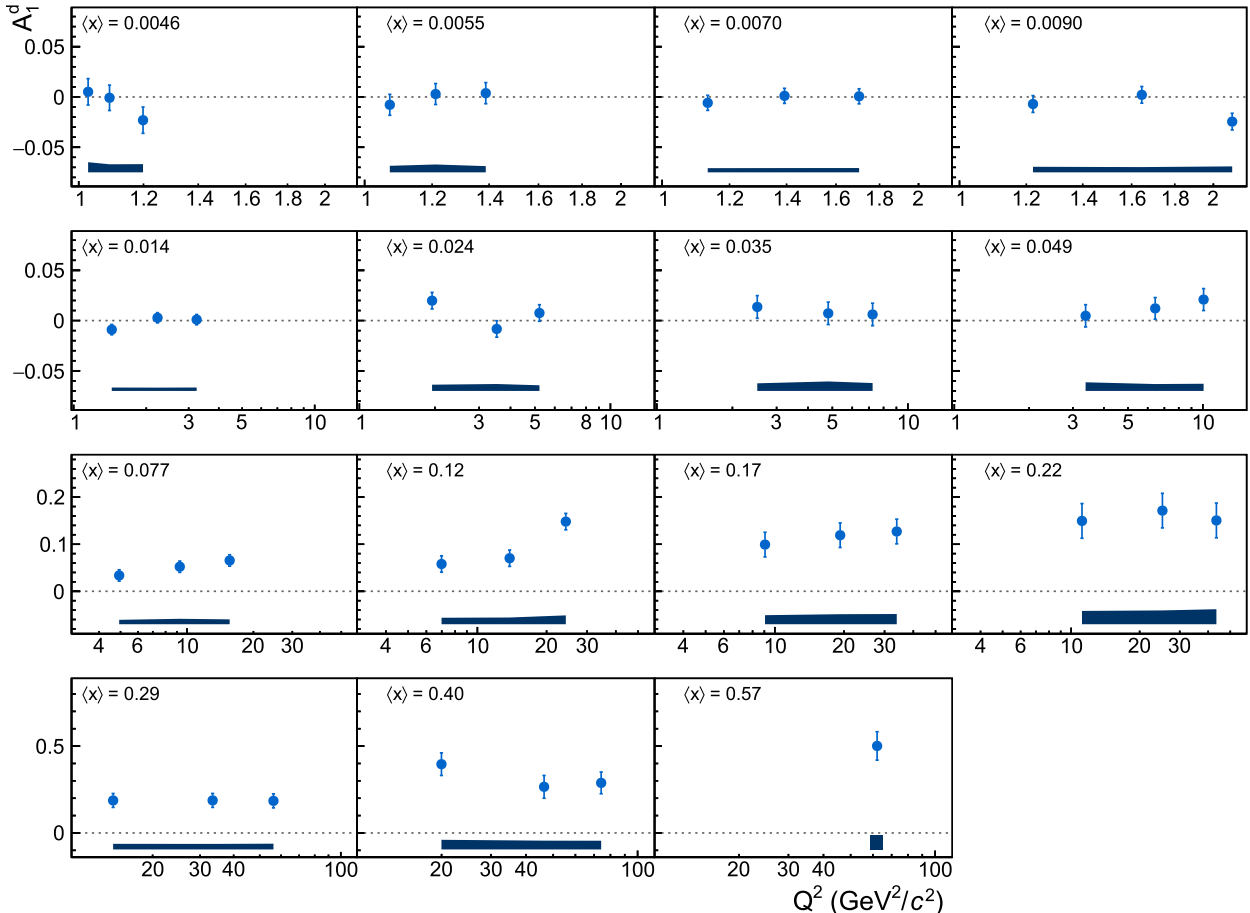


Fig. 3. Results on A_1^d from the combined COMPASS data in bins of x and Q^2 .

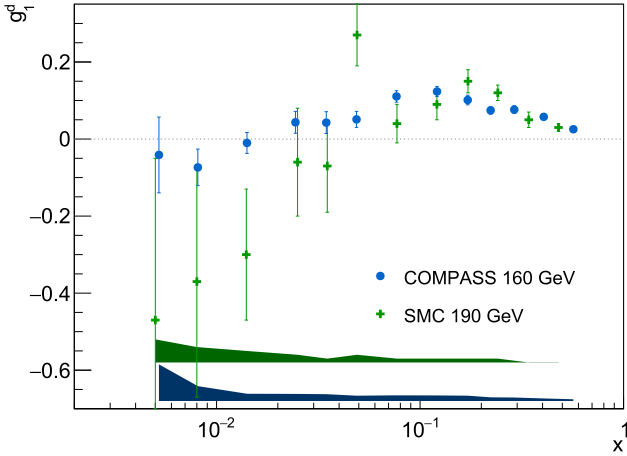


Fig. 4. Comparison between SMC [2] and combined COMPASS results on g_1^d . The systematic uncertainty is illustrated by the bands at the bottom. All data points are shown at their measured Q^2 values.

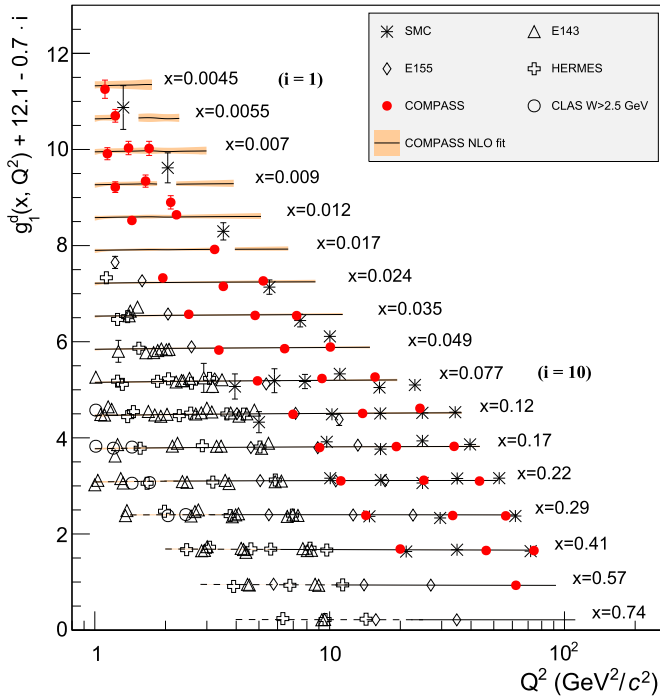


Fig. 5. World data on the spin-dependent structure function g_1^d as a function of Q^2 for various values of x with the combined COMPASS data as filled circles. The lines represent the Q^2 dependence for each value of x as determined from the updated NLO QCD fit to the world data. The dashed parts represent the region with $W^2 < 10 \text{ (GeV/c)}^2$.

persede the ones published in Ref. [7]. They improve the statistical precision of the combined world data on g_1^d , in particular at low x where SMC is the only other experiment that contributes.

The NLO QCD fit on the g_1 world data described in detail in Ref. [9] is repeated using the updated results for g_1^d . The fit results are shown as curves in Fig. 5 for the various x bins. Compared to the previous analysis, the changes in central values of resulting parameters are of the order of statistical uncertainties. The parameters of the QCD fit are available together with the deuteron results on HepData [21].

The presented final g_1^d values together with the final COMPASS results on g_1^p [8,9] are used to re-evaluate the Bjorken sum rule as described in the same reference. The results

Table 2

Contributions to Γ_1^N at $Q^2 = 3 \text{ (GeV/c)}^2$ with statistical uncertainties from the COMPASS data.

x range	Γ_1^N
$0 < x < 0.004$	-0.0015 ± 0.001
$0.004 < x < 0.7$	0.045 ± 0.002
$0.7 < x < 1.0$	0.001

$$\Gamma_1^{NS} = 0.192 \pm 0.007_{\text{stat}} \pm 0.015_{\text{sys}} \quad \text{and}$$

$$|g_A/g_V| = 1.29 \pm 0.05_{\text{stat}} \pm 0.10_{\text{sys}} \quad (8)$$

agree within statistical errors with the previously published ones.

The new combined data are also used to update the results for the first moment of the spin-dependent structure function of the nucleon, $\Gamma_1^N(Q^2) = \int_0^1 g_1^d(x, Q^2)/(1 - 1.5\omega_D)dx$. Here $\omega_D = 0.05 \pm 0.02$ [22] is the correction for the D-state admixture in the deuteron. The first moment is calculated by evolving the values of g_1^d to the common value $Q^2 = 3 \text{ (GeV/c)}^2$. From these values the contribution to the first moment from the measured x range is calculated. The contributions from the unmeasured regions are estimated using the parameterisations of parton distributions from our NLO QCD analysis [9]. For the region $0 < x < 0.004$ the contribution lies between -0.0015 and 0.001 . Such a small contribution can be expected as g_1^d is consistent with zero for $x < 0.02$. It is also consistent with zero at scales $Q^2 < 1 \text{ (GeV/c)}^2$ where the measurements extend to even lower values of x [11]. For the region $0.7 < x < 1$ the contribution to the first moment of g_1^d is as small and equal to 0.001 . The contributions from the different x ranges are shown in Table 2. The updated value of the first moment from COMPASS data alone is:

$$\Gamma_1^N(Q^2 = 3 \text{ (GeV/c)}^2) = 0.046 \pm 0.002_{\text{stat}} \pm 0.004_{\text{syst}} \pm 0.005_{\text{evol}}. \quad (9)$$

The systematic uncertainty contains the bin-to-bin correlated uncertainties of P_B , P_T , f , D , ω_D and F_2 . The uncertainties of P_B and P_T dominate, while the impact of possible false asymmetries largely cancels in the discussed integral. An uncertainty of 100% is used for the contribution from the large- x extrapolation, while for the low- x extrapolation the uncertainty is taken as half of the full range, i.e. 0.00125 . Both are included in the evolution uncertainty.

All presently available experimental information supports the observation that g_1^d vanishes when x decreases down to the lowest accessible values. As can be seen in Fig. 6, the first moment of g_1^d measured from only the COMPASS deuteron data approaches its asymptotic value already in the experimentally accessible region for $Q^2 = 3 \text{ (GeV/c)}^2$. It can hence be used for physics interpretation without using proton data and without invoking the Bjorken sum rule.

The structure function g_1^d as physical observable is factorisation-scheme independent, whereas its representation as convolution(s) of quark, anti-quark, and gluon helicity distributions with respective Wilson coefficient functions [23,24] involves a possible scheme dependence. In the ‘modified minimal subtraction’ ($\overline{\text{MS}}$) factorisation scheme [25], the first moment of the gluon coefficient function vanishes, and hence the first moment Γ_1^d does not depend on the gluon helicity distribution. This allows for the direct determination of the flavour-singlet axial charge a_0 from the COMPASS Γ_1^d result using only the axial charge a_8 as an additional input:

$$a_0(Q^2) = \frac{1}{\Delta C_S^{\overline{\text{MS}}}(Q^2)} \left[9\Gamma_1^N - \frac{1}{4}a_8\Delta C_{\text{NS}}^{\overline{\text{MS}}}(Q^2) \right] \quad (10)$$

Here, $\Delta C_S^{\overline{\text{MS}}}(Q^2)$ and $\Delta C_{\text{NS}}^{\overline{\text{MS}}}(Q^2)$ are the singlet and non-singlet coefficient functions, which are calculated in perturbative QCD in Ref. [26,27]. In the $\overline{\text{MS}}$ factorisation scheme, a_0 is identified with the total quark contribution to the nucleon spin: $a_0^{\overline{\text{MS}}} = \Delta\Sigma = (\Delta u + \Delta\bar{u}) + (\Delta d + \Delta\bar{d}) + (\Delta s + \Delta\bar{s})$. Here, $\Delta f^{(-)}$ is the first moment of helicity distribution of flavour- f quarks. Assuming SU(3) flavour symmetry, the value $a_8 = 0.585 \pm 0.025$ [28] is used. With $\alpha_s = 0.337 \pm 0.012$ for $Q^2 = 3(\text{GeV}/c)^2$ and the corresponding NLO value for $\Delta C_S^{\overline{\text{MS}}}(Q^2) = \Delta C_{\text{NS}}^{\overline{\text{MS}}}(Q^2) = 0.893$ the flavour-singlet axial charge is obtained using Γ_1^N as obtained in Eq. (9):

$$a_0(Q^2 = 3(\text{GeV}/c)^2) = 0.32 \pm 0.02_{\text{stat}} \pm 0.04_{\text{syst}} \pm 0.05_{\text{evol}}. \quad (11)$$

The largest contribution to the total uncertainty originates from the uncertainties in the evolution of g_1^d to a common value of Q^2 . This is due to the large uncertainty of the polarised gluon

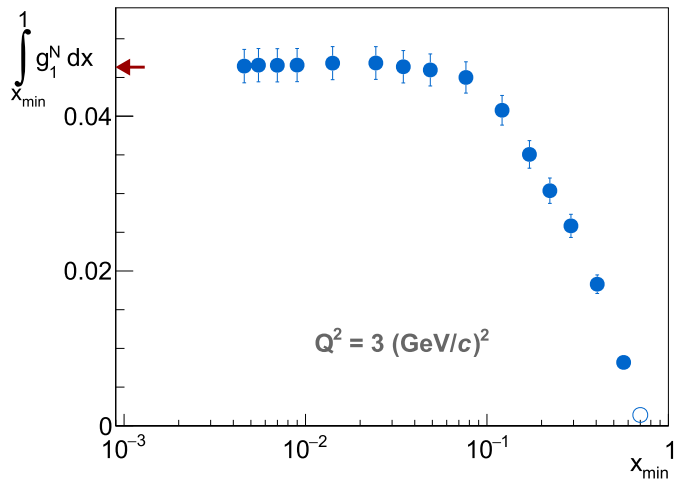


Fig. 6. Values of $\int_{x_{\min}}^1 g_1^d/(1-1.5\omega_D)dx$ as a function of x_{\min} . The open circle at $x = 0.7$ is obtained from the fit. The arrow on the left side shows the value for the full range, $0 \leq x \leq 1$.

distribution obtained in the fits. The extrapolation uncertainty is given by the extrapolation uncertainty of Γ_1^N as explained above, and is included in the evolution uncertainty. This independent result on a_0 is consistent with the value of a_0 obtained from the COMPASS NLO QCD fit [9] of the world data. Note the remarkably good statistical and systematic accuracy of this result obtained from only the COMPASS deuteron data when comparing to the corresponding accuracy of the fit result [9].

5. Summary and conclusions

We have presented new results on the longitudinal spin structure function g_1^d from data taken in 2006 and we have combined this data with our previous measurements. All data were taken using the 160 GeV CERN muon beam and a longitudinally polarised ^6LiD target. The results cover the kinematic range $0.004 < x < 0.7$, $1(\text{GeV}/c)^2 < Q^2 < 100(\text{GeV}/c)^2$ and $W > 4\text{GeV}/c^2$. The double-spin asymmetry is studied in bins of x and Q^2 . The combined results for g_1^d at low x ($x < 0.03$) improve considerably the precision compared to the only existing result in this region, which originates from SMC. Now, g_1^d appears consistent with zero at the presently lowest accessible values of x . The combined set of data was included in our NLO QCD fit to the g_1^p , g_1^d and g_1^n world data. In addition, a re-evaluation of the Bjorken sum rule was performed using only COMPASS results. Both for the QCD NLO fit and the Bjorken sum rule, the new values stay compatible with the published ones within statistical uncertainties. The analysis of the COMPASS deuteron data alone leads to a NLO determination of the flavour-singlet axial charge $a_0 = 0.32 \pm 0.02_{\text{stat}} \pm 0.04_{\text{syst}} \pm 0.05_{\text{evol}}$ at $Q^2 = 3(\text{GeV}/c)^2$ from the first moment of g_1^d . Together with the results on the proton spin structure function g_1^p [8,9], the results for g_1^d constitute the COMPASS legacy on the measurements of g_1 .

Acknowledgements

We gratefully acknowledge the support of the CERN management and staff and the skill and effort of the technicians of our collaborating institutes. This work was made possible by the financial support of our funding agencies.

Appendix A. Appendix

The results for A_1^d and g_1^d are given in Tables A.1 and A.2.

Table A.1

Values for A_1^d and g_1^d as a function of x at the measured values of Q^2 for the combined 2002–2006 data. The first uncertainty is statistical, the second one is systematic.

x range	$\langle x \rangle$	$\langle Q^2 \rangle ((\text{GeV}/c)^2)$	A_1^d	g_1^d
0.004–0.005	0.0046	1.10	$-0.0054 \pm 0.0074 \pm 0.0048$	$-0.13 \pm 0.17 \pm 0.11$
0.005–0.006	0.0055	1.22	$0.0003 \pm 0.0058 \pm 0.0043$	$0.00 \pm 0.12 \pm 0.09$
0.006–0.008	0.0070	1.39	$-0.0011 \pm 0.0042 \pm 0.0023$	$-0.016 \pm 0.071 \pm 0.040$
0.008–0.010	0.0090	1.62	$-0.0087 \pm 0.0049 \pm 0.0031$	$-0.121 \pm 0.064 \pm 0.038$
0.010–0.020	0.0141	2.19	$-0.0011 \pm 0.0032 \pm 0.0024$	$-0.010 \pm 0.027 \pm 0.019$
0.020–0.030	0.0244	3.29	$0.0075 \pm 0.0048 \pm 0.0034$	$0.043 \pm 0.028 \pm 0.018$
0.030–0.040	0.0346	4.43	$0.0095 \pm 0.0064 \pm 0.0042$	$0.043 \pm 0.028 \pm 0.018$
0.040–0.060	0.0487	6.06	$0.0159 \pm 0.0063 \pm 0.0044$	$0.051 \pm 0.021 \pm 0.014$
0.060–0.100	0.0766	9.00	$0.0527 \pm 0.0070 \pm 0.0072$	$0.111 \pm 0.015 \pm 0.015$
0.100–0.150	0.121	13.5	$0.095 \pm 0.010 \pm 0.011$	$0.123 \pm 0.013 \pm 0.014$
0.150–0.200	0.171	18.6	$0.121 \pm 0.015 \pm 0.016$	$0.101 \pm 0.013 \pm 0.014$
0.200–0.250	0.222	23.8	$0.160 \pm 0.022 \pm 0.020$	$0.0744 \pm 0.0096 \pm 0.0096$
0.250–0.350	0.290	31.1	$0.190 \pm 0.023 \pm 0.022$	$0.076 \pm 0.010 \pm 0.009$
0.350–0.500	0.405	43.9	$0.317 \pm 0.037 \pm 0.036$	$0.0576 \pm 0.0069 \pm 0.0067$
0.500–0.700	0.567	60.8	$0.494 \pm 0.082 \pm 0.084$	$0.0254 \pm 0.0042 \pm 0.0045$

Table A.2

Values for A_1^d and g_1^d as a function of x and Q^2 for the combined 2002–2006 data. The first uncertainty is statistical, the second one is systematic.

x range	$\langle x \rangle$	$\langle Q^2 \rangle ((\text{GeV}/c)^2)$	A_1^d	g_1^d
0.004–0.005	0.0045	1.03	$0.005 \pm 0.013 \pm 0.010$	$0.12 \pm 0.30 \pm 0.23$
0.004–0.005	0.0046	1.09	$-0.001 \pm 0.013 \pm 0.008$	$-0.02 \pm 0.29 \pm 0.19$
0.004–0.005	0.0047	1.20	$-0.023 \pm 0.013 \pm 0.008$	$-0.54 \pm 0.30 \pm 0.19$
0.005–0.006	0.0055	1.07	$-0.008 \pm 0.010 \pm 0.007$	$-0.15 \pm 0.20 \pm 0.12$
0.005–0.006	0.0055	1.21	$0.003 \pm 0.010 \pm 0.008$	$0.06 \pm 0.21 \pm 0.16$
0.005–0.006	0.0056	1.39	$0.004 \pm 0.011 \pm 0.006$	$0.08 \pm 0.22 \pm 0.14$
0.006–0.008	0.0069	1.13	$-0.0058 \pm 0.0075 \pm 0.0042$	$-0.09 \pm 0.11 \pm 0.06$
0.006–0.008	0.0069	1.39	$0.0011 \pm 0.0075 \pm 0.0043$	$0.02 \pm 0.12 \pm 0.07$
0.006–0.008	0.0072	1.70	$0.0007 \pm 0.0075 \pm 0.0043$	$0.01 \pm 0.13 \pm 0.07$
0.008–0.010	0.0089	1.22	$-0.0070 \pm 0.0084 \pm 0.0055$	$-0.08 \pm 0.10 \pm 0.07$
0.008–0.010	0.0089	1.65	$0.0021 \pm 0.0083 \pm 0.0052$	$0.03 \pm 0.11 \pm 0.07$
0.008–0.010	0.0091	2.11	$-0.0245 \pm 0.0083 \pm 0.0059$	$-0.36 \pm 0.12 \pm 0.09$
0.010–0.020	0.0132	1.44	$-0.0090 \pm 0.0051 \pm 0.0034$	$-0.076 \pm 0.043 \pm 0.029$
0.010–0.020	0.0135	2.23	$0.0028 \pm 0.0051 \pm 0.0033$	$0.027 \pm 0.050 \pm 0.032$
0.010–0.020	0.0156	3.24	$0.0009 \pm 0.0051 \pm 0.0034$	$0.009 \pm 0.049 \pm 0.033$
0.020–0.030	0.0239	1.95	$0.0198 \pm 0.0082 \pm 0.0062$	$0.101 \pm 0.042 \pm 0.032$
0.020–0.030	0.0240	3.53	$-0.0083 \pm 0.0082 \pm 0.0069$	$-0.051 \pm 0.050 \pm 0.042$
0.020–0.030	0.0253	5.22	$0.0075 \pm 0.0082 \pm 0.0056$	$0.048 \pm 0.053 \pm 0.037$
0.030–0.040	0.0342	2.51	$0.014 \pm 0.011 \pm 0.008$	$0.052 \pm 0.043 \pm 0.029$
0.030–0.040	0.0344	4.82	$0.007 \pm 0.011 \pm 0.009$	$0.033 \pm 0.051 \pm 0.043$
0.030–0.040	0.0352	7.24	$0.006 \pm 0.011 \pm 0.008$	$0.029 \pm 0.054 \pm 0.038$
0.040–0.060	0.0477	3.38	$0.005 \pm 0.011 \pm 0.009$	$0.014 \pm 0.032 \pm 0.025$
0.040–0.060	0.0482	6.43	$0.012 \pm 0.011 \pm 0.007$	$0.040 \pm 0.036 \pm 0.023$
0.040–0.060	0.0502	10.1	$0.021 \pm 0.011 \pm 0.007$	$0.072 \pm 0.037 \pm 0.025$
0.060–0.100	0.0744	4.93	$0.034 \pm 0.012 \pm 0.009$	$0.067 \pm 0.024 \pm 0.019$
0.060–0.100	0.0757	9.28	$0.052 \pm 0.012 \pm 0.012$	$0.111 \pm 0.026 \pm 0.025$
0.060–0.100	0.0796	15.6	$0.065 \pm 0.012 \pm 0.010$	$0.140 \pm 0.026 \pm 0.022$
0.100–0.150	0.119	6.99	$0.058 \pm 0.017 \pm 0.014$	$0.072 \pm 0.022 \pm 0.017$
0.100–0.150	0.120	13.8	$0.070 \pm 0.017 \pm 0.014$	$0.092 \pm 0.023 \pm 0.019$
0.100–0.150	0.124	24.2	$0.148 \pm 0.017 \pm 0.019$	$0.191 \pm 0.023 \pm 0.025$
0.150–0.200	0.171	9.06	$0.099 \pm 0.026 \pm 0.019$	$0.082 \pm 0.022 \pm 0.016$
0.150–0.200	0.171	19.2	$0.119 \pm 0.026 \pm 0.021$	$0.101 \pm 0.022 \pm 0.018$
0.150–0.200	0.174	33.9	$0.127 \pm 0.026 \pm 0.022$	$0.106 \pm 0.022 \pm 0.018$
0.200–0.250	0.221	11.2	$0.150 \pm 0.037 \pm 0.028$	$0.087 \pm 0.022 \pm 0.017$
0.200–0.250	0.221	25.2	$0.171 \pm 0.037 \pm 0.029$	$0.100 \pm 0.021 \pm 0.017$
0.200–0.250	0.224	43.5	$0.151 \pm 0.037 \pm 0.032$	$0.085 \pm 0.021 \pm 0.018$
0.250–0.350	0.287	14.3	$0.187 \pm 0.040 \pm 0.032$	$0.071 \pm 0.015 \pm 0.012$
0.250–0.350	0.288	33.4	$0.187 \pm 0.040 \pm 0.032$	$0.068 \pm 0.015 \pm 0.012$
0.250–0.350	0.295	56.2	$0.185 \pm 0.040 \pm 0.033$	$0.062 \pm 0.014 \pm 0.011$
0.350–0.500	0.400	20.0	$0.396 \pm 0.065 \pm 0.056$	$0.070 \pm 0.012 \pm 0.010$
0.350–0.500	0.402	46.4	$0.266 \pm 0.066 \pm 0.051$	$0.043 \pm 0.011 \pm 0.008$
0.350–0.500	0.411	74.1	$0.288 \pm 0.063 \pm 0.050$	$0.041 \pm 0.009 \pm 0.007$
0.500–0.700	0.569	62.1	$0.501 \pm 0.082 \pm 0.084$	$0.0204 \pm 0.0033 \pm 0.0035$

References

- [1] EMC, J. Ashman, et al., Phys. Lett. B 206 (1988) 364, Nucl. Phys. B 328 (1989) 1.
- [2] SMC, B. Adeva, et al., Phys. Rev. D 58 (1998) 112001.
- [3] C. Alexandrou, Parton distribution functions from Lattice QCD, in: Proceedings of Light Cone 2015 Conference, Frascati, Italy, 2015, Few-Body Syst. 57 (2016) 621.
- [4] C.A. Aidala, S.D. Bass, D. Hasch, G.K. Mallot, Rev. Mod. Phys. 85 (2013) 655.
- [5] J. Blumlein, A. Vogt, Phys. Lett. B 370 (1996) 149, Phys. Lett. B 386 (1996) 350.
- [6] J. Bartels, B.I. Ermolaev, M.G. Ryskin, Z. Phys. C 70 (1996) 273, Z. Phys. C 72 (1996) 627.
- [7] COMPASS Collaboration, V.Yu. Alexakhin, et al., Phys. Lett. B 647 (2007) 8.
- [8] COMPASS Collaboration, M.G. Alekseev, et al., Phys. Lett. B 690 (2010) 466.
- [9] COMPASS Collaboration, C. Adolph, et al., Phys. Lett. B 753 (2016) 18.
- [10] M. Wilfert, PhD thesis, Mainz University, 2017.
- [11] COMPASS Collaboration, V.Yu. Alexakhin, et al., Phys. Lett. B 647 (2007) 330.
- [12] COMPASS Collaboration, P. Abbon, et al., Nucl. Instrum. Methods A 577 (2007) 455.
- [13] P. Hoodbhoy, R.L. Jaffe, A.V. Manohar, Nucl. Phys. B 312 (1989) 571.
- [14] HERMES Collaboration, A. Airapetian, et al., Phys. Rev. Lett. 95 (2005) 242001.
- [15] COMPASS Collaboration, E.S. Ageev, et al., Nucl. Phys. B 765 (2007) 31.
- [16] CLAS Collaboration, K.V. Dharmawardane, et al., Phys. Lett. B 641 (2006) 11.
- [17] HERMES Collaboration, A. Airapetian, et al., Phys. Rev. D 75 (2007) 012007.
- [18] E155 Collaboration, P.L. Anthony, et al., Phys. Lett. B 463 (1999) 339.
- [19] E143 Collaboration, K. Abe, et al., Phys. Rev. D 58 (1998) 112003.
- [20] E143 Collaboration, K. Abe, et al., Phys. Lett. B 452 (1999) 194.
- [21] The Durham HepData Project, <http://durpdg.dur.ac.uk/>.
- [22] R. Machleidt, et al., Phys. Rep. 149 (1987) 1.
- [23] G. Altarelli, R.D. Ball, S. Forte, G. Ridolfi, Nucl. Phys. B 496 (1997) 337.
- [24] R. Mertig, W.L. van Neerven, Z. Phys. C 70 (1996) 637.
- [25] W.A. Bardeen, A.J. Buras, D.W. Duke, T. Muta, Phys. Rev. D 18 (1978) 3998.
- [26] J. Kodaira, Nucl. Phys. B 165 (1980) 129.
- [27] A.L. Kataev, Phys. Rev. D 50 (1994) R5469.
- [28] Particle Data Group, C. Caso, et al., Eur. Phys. J. C 3 (1998) 1; Y. Goto, et al., Phys. Rev. D 62 (2000) 034017.